A new diagnostic for AMOC heat transport applied to the CESM large ensemble

C Spencer Jones[1], Scout Jiang[2]and Ryan P. Abernathey[2]

[1]Texas A&M University, College Station, TX

[2]Columbia University, New York, NY

Key Points:

- We introduce a new diagnostic for AMOC heat transport that partitions the flow into mass-conserving gyre and overturning components
- The new method is compared with the standard method that relies on zonally averaging the temperature and velocity fields
- The new method provides a clearer way of separating heat transport by the gyres and by the overturning

Corresponding author: C. Spencer Jones, `spencerjones@tamu.edu`

Abstract

Atlantic time-mean heat transport is northward at all latitudes and exhibits strong multidecadal variability between about 30°N and 55°N. Atlantic heat transport variability influences many aspects of the climate system, including regional surface temperatures, subpolar heat content, Arctic sea-ice concentration and tropical precipitation patterns. Atlantic heat transport and heat transport variability are commonly partitioned into two components: the heat transport by the AMOC and the heat transport by the gyres. In this paper we compare three different methods for performing this partition, and we apply these methods to the CESM1 Large Ensemble at 34°N, 26°N and 5°S. We discuss the strengths and weaknesses of each method. One of these methods is a new physically-motivated method based on the pathway of the northward-flowing part of AMOC. This paper presents a preliminary version of our method. This preliminary version works only when the AMOC follows the western boundary of the basin. In this context, the new method provides a sensible estimate of heat transport by the overturning and by the gyre, and it is easier to interpret than other methods. According to our new diagnostic, at 34°N and at 26°N AMOC explains 120% of the multidecadal variability (20% is compensated by the gyre), and at 5°S AMOC explains 90% of multidecadal variability.

Plain Language Summary

Scientists often want to quantify how much heat is transported by the Atlantic Meridional Overturning Circulation (sometimes called the "Conveyor Belt" circulation) and how much heat is transported by the ocean's gyres. This paper compares some different methods for estimating the heat transport by the overturning circulation and by the gyres, including a new method that has not been used before. While previous methods are easier to apply to observations, the new method gives results that are easier to understand.

1 Introduction

The Atlantic Meridional Overturning Circulation (AMOC) comprises northward flow of warmer water near the surface, deep water formation in the North Atlantic, and southward flow of cooler water at depth. The AMOC transports heat northward throughout the Atlantic basin, warming the Northern Hemisphere (Jackson et al., 2015; Buckley & Marshall, 2016) and performing 20% of the total planetary poleward heat trans-

port at 26.5°N (Trenberth & Fasullo, 2017). The AMOC's cross-equatorial heat transport shifts the intertropical convergence zone (ITCZ) northward, affecting precipitation patterns close to the equator (Kang et al., 2009; Marshall et al., 2014).

Variations in northward Atlantic heat transport are thought to be a key driver of Atlantic Multidcadal Variability (Oldenburg et al., 2021), which affects variability in multiple parts of the climate system (Zhang et al., 2019), including tropical precipitation (Folland et al., 1986; Martin & Thorncroft, 2014), Atlantic hurricane frequency (Goldenberg et al., 2001; Klotzbach et al., 2015), and North Atlantic sea ice variability (Yeager et al., 2015). Low frequency ocean variability is a source of predictability in the climate system, meaning that parts of the climate system that are driven by AMOC variability may be predictable using observations of the ocean (Borchert et al., 2018). AMOC low-frequency variability and Atlantic decadal predictability vary significantly between climate models (Yan et al., 2018). To understand the cause of differences between models, it is helpful to characterize how the AMOC and the gyres interact to influence northward ocean heat transport. In this paper, we use three different methods to estimate how much ocean heat transport is performed by AMOC.

Many studies have attempted to separate the heat transport by the overturning circulation from the heat transport by the gyres (e.g. Bryan (1962); Hall and Bryden (1982); McDonagh et al. (2010); Ferrari and Ferreira (2011); Piecuch et al. (2017)). Most studies suggest that AMOC is the primary driver of heat transport in the subtropical gyre region and that the gyre is a more important driver in the subpolar gyre region (Eden & Willebrand, 2001; Piecuch et al., 2017). Many of the studies that have partitioned the heat transport by the gyres and the heat transport by the overturning circulation have done so with the goal of identifying how much of the heat transport variability is driven by wind and how much is driven by buoyancy forcing. AMOC variability is often thought to be primarily driven by buoyancy forcing, and the gyres are thought to be primarily driven by wind forcing. But recent studies have shown that gyre strength is strongly influenced by buoyancy forcing (Bhagtani et al., 2023), and that AMOC strength is strongly influenced by wind forcing (Yang, 2015; Cessi, 2018). The goal of this study is not to partition the heat transport caused by wind from the heat transport caused by buoyancy forcing, but to elucidate how the total AMOC transport influences heat transport at multiple latitudes, and to clarify whether this heat transport takes place on the western boundary or in the interior of the basin.

Most previous studies define the heat transport by the overturning as the zonal integral of the volume transport multiplied by the zonal mean temperature, integrated in the vertical. In all the studies that use this method, the integrals are taken in depth space. In the last twenty years or so, oceanographers have started to define the AMOC using a zonal-average in density space (Foukal & Chafik, 2022). Recent work by Zhang and Thomas (2021) has shown that flows on the same depth level in the subpolar gyre region have different densities and form part of the AMOC. It is clear that the old depth-averaged way of looking at things can still be useful, but much progress has been made by looking at the AMOC in new ways.

In this work, we introduce a new method for partitioning the heat transport due to the overturning and the heat transport due to the gyres based on a more nuanced understanding of the circulation patterns. Northward flow in the North Atlantic is dominated by the Gulf Stream. The Gulf Stream is significantly stronger than required to satisfy Sverdrup balance (Gray & Riser, 2014), which can partly be attributed to the presence of an additional flow component: the northward component of the AMOC. AMOC transport primarily follows the western boundary at latitudes where the gyre is clockwise (Stommel, 1957). Rypina et al. (2011) showed that drifters in the far west of the Gulf Stream are likely to reach the North Atlantic, whereas drifters further to the east are unlikely to cross northward into latitudes associated with the subpolar gyre. In this work we extend this idea, splitting the upper part of the ocean into AMOC transport, which follows the western boundary, and gyre transport, which occupies the interior.

Our method is conceptually similar to a method used by Roemmich and Wunsch (1985). Roemmich and Wunsch (1985) estimated the temperature transport in the deep ocean, the temperature transport in the western boundary current, and the temperature transport in the southward flowing part of the gyre from observations. Talley (1999) used a similar method. These authors took the mean temperature in the western boundary current and calculated the heat transport by the AMOC to be the volume transport of the AMOC multiplied the difference in temperature between the western boundary current and the deep ocean. They applied their method to sections at 24°N and found that 90% of the mean northward heat transport is performed by the AMOC at this latitude, and they commented that the northward heat transport is dominated by the AMOC across multiple years of observations. Because our new method is applied to a model, we are able to more clearly define the regions associated with the AMOC and with the gyre.

In this work, we compare three methods for partitioning ocean heat transport into heat transport by the overturning and heat transport by the gyres. We use the CESM large ensemble as a testbed for these different methods, because the existence of long runs and many ensemble members allows us to examine variability at multiple timescales. The CESM large ensemble is described in section 2 and the three methods for partitioning heat transport by the overturning and heat transport by the gyres are described in section 2.1. Sections 3.1 and 3.2 describe the total AMOC and heat transport variability in the CESM large ensemble, and section 3.3 shows the results of different methods for partitioning the heat transport by the overturning and the heat transport by the gyres. Section 4 discusses the results and presents conclusions.

2 Methods

We explore these diagnostics in the context of ocean models, where the time varying circulation and temperature fields are perfectly known. Our analysis uses a large ensemble of ocean simulation in order to sample broadly the modes of natural variability of the North Atlantic circulation. The CESM Large Ensemble is a group of simulations performed using a 1° nominal resolution fully-coupled version of the Community Earth System Model (CESM1) (Kay et al., 2015). Forty ensemble members were created for the period 1920-2100. Each ensemble member has the same radiative forcing scenario, but the initial atmospheric temperature is perturbed with a spatially random perturbation order 10^{-14}K. As a result of internal variability, each ensemble member's state follows a unique trajectory with different regional temperature patterns and different AMOC variability.

We used the cloud-optimized dataset, which is stored on Amazon Web Services (AWS) thanks to the AWS Public Dataset Program (de La Beaujardiere et al., 2019). In this work we used the first 35 ensemble members for the period 1940-2005. 1940 is chosen because this allows time for the internal variability of the system to diverge, so that the ensemble members are different from each other throughout the chosen period. 2005 is a natural end date, because it marks the end of the historical runs for the CESM1 Large Ensemble. During the period 1940-2005 multidecadal variability dominates over long-term trends in AMOC and heat transport. Members of the CESM large ensemble are not meant to have exactly the same variability as the real world, but to represent the range of possible internal variability. Many of the ensemble members exhibit North At-

lantic subpolar gyre ocean heat content variability with similar magnitude to ECCOv4r3 (not shown).

2.1 Separating heat transport by the gyre from heat transport by the overturning circulation

Heat transport by each gyre is primarily wind driven, and is likely to have short time scales and spatial effects that are confined to that gyre. Heat transport by the overturning is both wind and buoyancy driven, and is more likely to impact temperatures in the far North Atlantic. Hence, it is desirable to partition the heat transport across a particular latitude into the heat transport by the overturning and the heat transport by the gyres. All the methods described in this section are designed to be applied at a fixed latitude. The notion of heat transport by the flow across a section is only well-defined when the net mass transport (or volume transport, in a Boussinesq ocean model) of the flow is zero (see e.g. Warren (1999); Boccaletti et al. (2005); Pickart and Spall (2007)). In the Atlantic basin, there is a net southward volume transport of about 1 Sv, and the heat transported by this net throughflow is dependent on our choice of reference temperature. We still remove the net throughflow component of the heat transport. Because the net throughflow is small, the results of this study are relatively insensitive to the choice of reference temperature.

At each latitude, we remove the mean velocity from the total velocity to find the volume conserving part of the velocity,

$$v_{vc}(x,z,t) = v(x,z,t) - \overline{v}(t)\,, \tag{1}$$

where

$$\overline{v}(t) = \frac{\int_{-H}^{0}\int_{x_w}^{x_e} v(x,z,t)\,dx\,dz}{\int_{-H}^{0}\int_{x_w}^{x_e} dx\,dz}\,, \tag{2}$$

and x is distance in the longitudinal direction, z is distance in the vertical, v is the meridional velocity, H is the ocean depth, x_w is the western boundary of the Atlantic and x_e is the eastern boundary of the Atlantic. Ideally, the residual velocity (including the eddy transport) would be used in these calculations, but this data was not readily available, so the effects of parameterized eddies are not included in v. We also remove the southward heat transport that is associated with the mean velocity, so

$$\mathrm{OHT}_{vc}(t) = \int_{-H}^{0}\int_{x_w}^{x_e} v(x,z,t)\theta(x,z,t)\,dx\,dz - \int_{-H}^{0}\int_{x_w}^{x_e} \theta(x,z,t)\overline{v}(t)\,dx\,dz\,, \tag{3}$$

where θ is temperature.

The total volume conserving heat transport, OHT_{vc}, can be further decomposed into the sum of heat transport by multiple sub-flows, provided that each sub-flow has no net mass transport associated with it. There are infinitely many possible such decompositions. Once the net velocity and associated heat transport have been removed, we apply and compare three methods for separating the heat transport by the overturning and the heat transport by the gyres. These methods are illustrated in figure 1. The first method, which we call the zonal-mean method in z-space, has been in use for a long time (Bryan, 1962; Hall & Bryden, 1982; McDonagh et al., 2010; Piecuch et al., 2017). In this method the heat transport by the overturning, $\mathrm{OHT}^{(z)}_{ot}(t)$, is calculated by multiplying the zonally-integrated velocity by the zonal-mean temperature, where all the zonal integrals are taken at constant depth, and then integrating in the vertical, so

$$\mathrm{OHT}^{(z)}_{ot}(t) = \int_{-H}^{0} \left(\int_{x_w}^{x_e} v(x,z,t)\,dx \right) \left(\frac{\int_{x_w}^{x_e} \theta(x,z,t)\,dx}{\int_{x_w}^{x_e} dx} \right) dz\,, \tag{4}$$

as illustrated in the top panel to figure 1. In this method, the heat transport by the gyre is the total volume-conserving heat transport minus the heat transport by the overturning,

$$\mathrm{OHT}^{(z)}_{gyre}(t) = \mathrm{OHT}_{vc}(t) - \mathrm{OHT}^{(z)}_{ot}(t)\,, \tag{5}$$

where $\mathrm{OHT}^{(z)}_{ot}(t)$ is the heat transport attributed to the AMOC by the zonal-mean method in z-space and $\mathrm{OHT}^{(z)}_{gyre}(t)$ is the heat transport attributed to the gyre by the zonal-mean method in z-space.

The second method we investigate is similar to the first method, but zonal integrals are taken in density coordinates instead of depth coordinates. Thickness-weighting is necessary to preserve volume conservation (see e.g. Young (2012)), so

$$\begin{aligned} \mathrm{OHT}^{(\rho)}_{ot}(t) &= \int_{\rho_{min}}^{\rho_{max}} \left(\int_{x_w}^{x_e} v(x,\rho,t)\zeta_{\tilde{\rho}}(x,\rho,t)\,dx \right) \left(\frac{\int_{x_w}^{x_e} \theta(x,\rho,t)\zeta_{\tilde{\rho}}(x,\rho,t)\,dx}{\int_{x_w}^{x_e} \zeta_{\tilde{\rho}}(x,\rho,t)\,dx} \right) d\rho\,, \quad (6) \\ &\approx \sum_{\rho} \left(\int_{x_w}^{x_e} v(x,\rho,t)\delta z(x,\rho,t)\,dx \right) \left(\frac{\int_{x_w}^{x_e} \theta(x,\rho,t)\delta z(x,\rho,t)\,dx}{\int_{x_w}^{x_e} \delta z(x,\rho,t)\,dx} \right), \quad (7) \end{aligned}$$

where ζ is the depth of a density surface and $\zeta_{\tilde{\rho}}$ is the derivative of ζ with respect to density. When this calculation is discretized, a finite layer thickness δz is used to describe the vertical distance between two isopycnals, and we sum over all densities. This method is illustrated in the second panel of figure 1. As in the first method, the heat transport by the gyre is the total volume-conserving heat transport minus the heat transport by

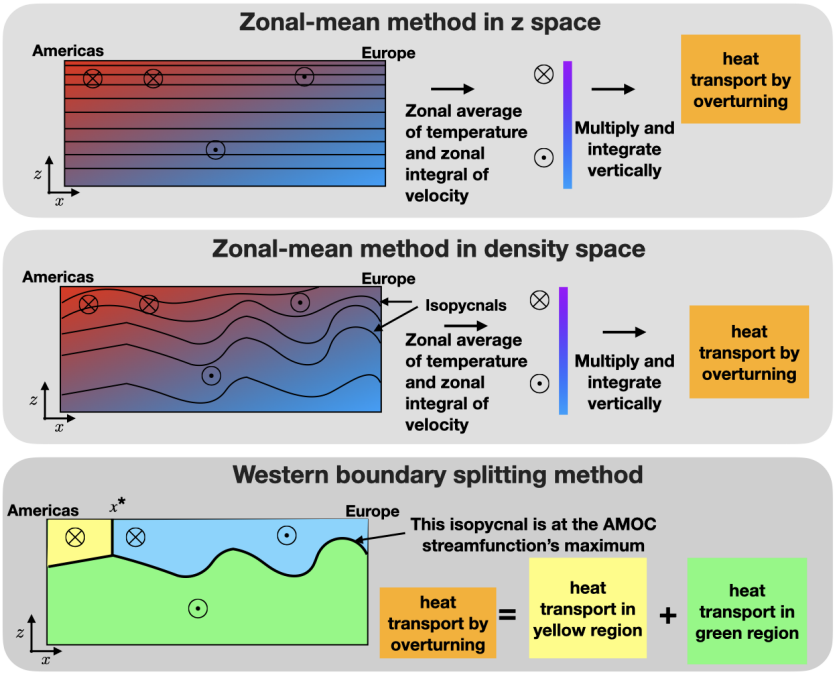

Figure 1. Schematic of three different methods for separating heat transport due to the overturning and heat transport due to the gyre.

the overturning,

$$\mathrm{OHT}^{(\rho)}_{gyre}(t) = \mathrm{OHT}_{vc}(t) - \mathrm{OHT}^{(\rho)}_{ot}(t)\,, \tag{8}$$

where $\mathrm{OHT}^{(\rho)}_{ot}(t)$ is the heat transport attributed to the AMOC by the zonal-mean method in density-space and $\mathrm{OHT}^{(\rho)}_{gyre}(t)$ is the heat transport attributed to the gyre by the zonal-mean method in density-space.

Our new method is motivated by the pathway of water in the northward limb of the AMOC, as illustrated by the pseudo-streamfunction (Jones & Cessi, 2018), which is plotted in figure 2,

$$\Phi = \int_{x_w}^{x}\int_{-H}^{0} v\mathcal{H}(\rho-\rho_m)\,\mathrm{dz}\,\mathrm{dx}'\,, \tag{9}$$

where $\mathcal{H}$ is the Heaviside function and ρ_m is the isopycnal that passes through the maximum of the meridional overturning streamfunction (the yellow dashed-dotted line in figure 3).

As shown in figure 2, the AMOC's northward branch winds around the gyres, following the red contours northward. The blue contours in figure 2 represent the gyres. We expect that the strength of the gyres is independent of the strength of AMOC at long

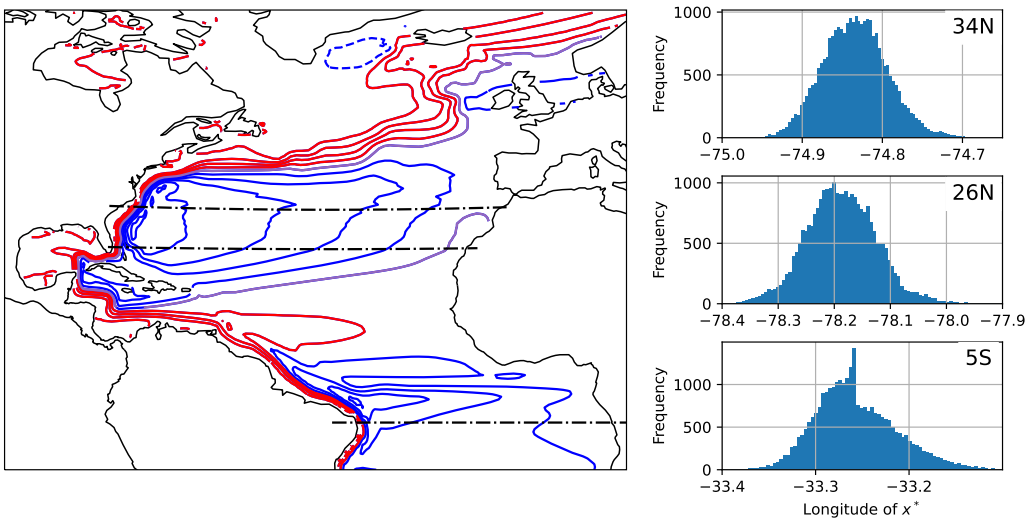

Figure 2. The red, blue and purple contours in the left panel show the pseudostreamfunction, the mean transport above $\sigma_0 = 27.74$ (an isopycnal that passes through the maximum MOC streamfunction, as shown by the horizontal yellow line in figure 3) integrated from the western boundary eastward. The contour interval is 5 Sv. Red contours are contours that start in the south and end in the north, representing the AMOC. Blue contours are coutours that cross each latitude twice, representing the gyres. The black dashed-dotted lines show the three latitudes used in this study. The right three panels are histograms of the location of x^*, the longitude that divides the AMOC transport and the gyre transport in the streamfunction splitting method (see the third panel of figure 1).

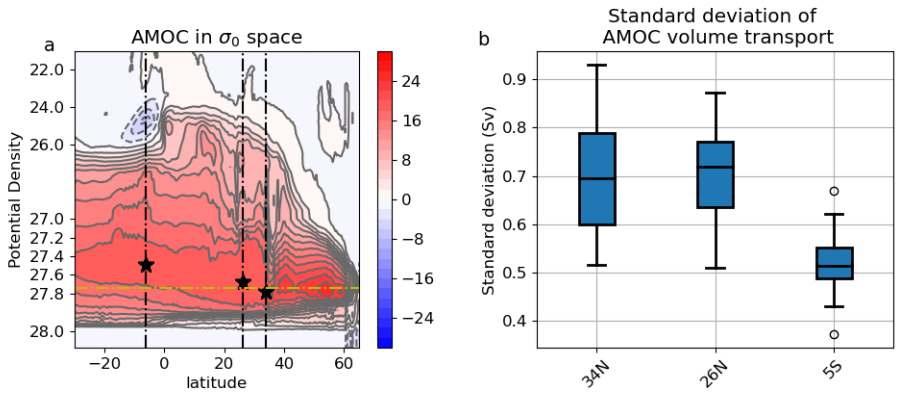

Figure 3. a) The Atlantic meridional overturning circulation in potential density space. b) The standard deviation of the AMOC volume transport at 34°N, 26°N and 5°S

timescales, and that the gyres are primarily driven by the wind, although recirculation of northward AMOC transport may also be present.

Because the circulation is three-dimensional, the total transport above density surface ρ_m contains a small divergent component, and Φ is not a traditional streamfunction. A small number of open contours like the purple contour in figure 2 do not originate in the far south. These contours represent the movement of water that upwelled across ρ_m within the domain.

In general, the red contours that represent the AMOC occupy the western boundary only at latitudes with clockwise gyre circulation. In this paper, we focus on these latitudes, because the AMOC pathway does not move around very much at these latitudes. We plan to extend the method to other latitudes in future.

In our new method, which we call the streamfunction splitting method, a constant-latitude section is divided into three regions. The first region is the deep region: this region is defined as the area below the dividing isopycnal, the green region in the bottom panel of figure 1. This dividing isopycnal is chosen to be the isopycnal that passes through the maximum of the meridional overturning streamfunction at that latitude (see stars in figure 3a). The second region is the western-boundary region, the yellow region in the bottom panel of figure 1, which is defined as the region above the dividing isopycnal and west of the latitude x^*. Latitude x^* is chosen such that the volume transport through the deep (green) region plus the volume transport through the western boundary (yellow) region sums to zero. The third region is the gyre region, the light blue region in the bottom panel of figure 1, and this region is defined to be above the dividing isopycnal and east of x^*. By definition, the volume transport through the gyre region is zero.

Here, we apply the streamfunction splitting method to the meridional velocity field after performing a 24-month rolling time average in density space. Without this time-average, x^* moves around a lot and sometimes is not defined. The dividing longitude x^* is shown in the right panels figure 2 at each latitude. Note that x^* is close to the western boundary in all cases, meaning that there is strong northward flow in the western boundary current that is associated with AMOC.

Using a running mean that is applied after the heat transport is partitioned into heat transport by the overturning and heat transport by the gyres, we further separate

the heat transport variability into variability on 2-10yr timescales and variability on 10+ year timescales. Ten years is chosen for ease of comparison with previous studies (e.g. Larson et al. (2020)).

3 Results

3.1 AMOC variability in the CESM large ensemble

AMOC variability is one cause of inter-decadal heat transport variability. Figure 3a shows the mean MOC as a function of density in the CESM large ensemble: the depth and mean strength of the MOC does not vary much between ensemble members. The mean AMOC volume transport is about 20 Sv.

Figure 3a shows the standard deviation of the smoothed AMOC volume transport at three different latitudes. The latitude 34°N is chosen because it is the most northerly latitude before the Gulf Stream separates in observations. In CESM1, the Gulf Stream separation latitude is further north than Cape Hatteras, but we have chosen to use 34°N because this is the most northerly latitude where the western boundary current compares well with observations. The latitude 26°N is chosen because it is the location of the RAPID array. 34°N and 26°N are relatively close together, and we expect the results at these latitudes to be relatively similar. 5°S was chosen to examine AMOC transport variability near to the equator. AMOC variability is generally larger at 34°N and 26°N than at 5°S, as shown in figure 3b, so we expect that AMOC-driven heat transport variability will be larger at 34°N and 26°N than at 5°S.

3.2 Heat transport variability in the CESM large ensemble

Figure 4a-c shows the timeseries of heat and AMOC transport at the three chosen latitudes for the third ensemble member, which is chosen as a representative ensemble member. Heat transport is strongly correlated with AMOC at all three latitudes and for both timescales of variability shown here (orange and blue lines in 4a-c).

Figure 4d-e shows the correlation between AMOC transport and heat transport at the three chosen latitudes for all ensemble members, plotted as a function of the standard deviation of AMOC strength. Values further to the right have more AMOC variability and values further up have larger correlations between AMOC and AMOC heat transport. Both AMOC variability and its correlation with heat transport are stronger

at 34°N and 26°N than at 5°S on 2-10yr timescales (figure 4d) and on 10+yr timescales (figure 4e).

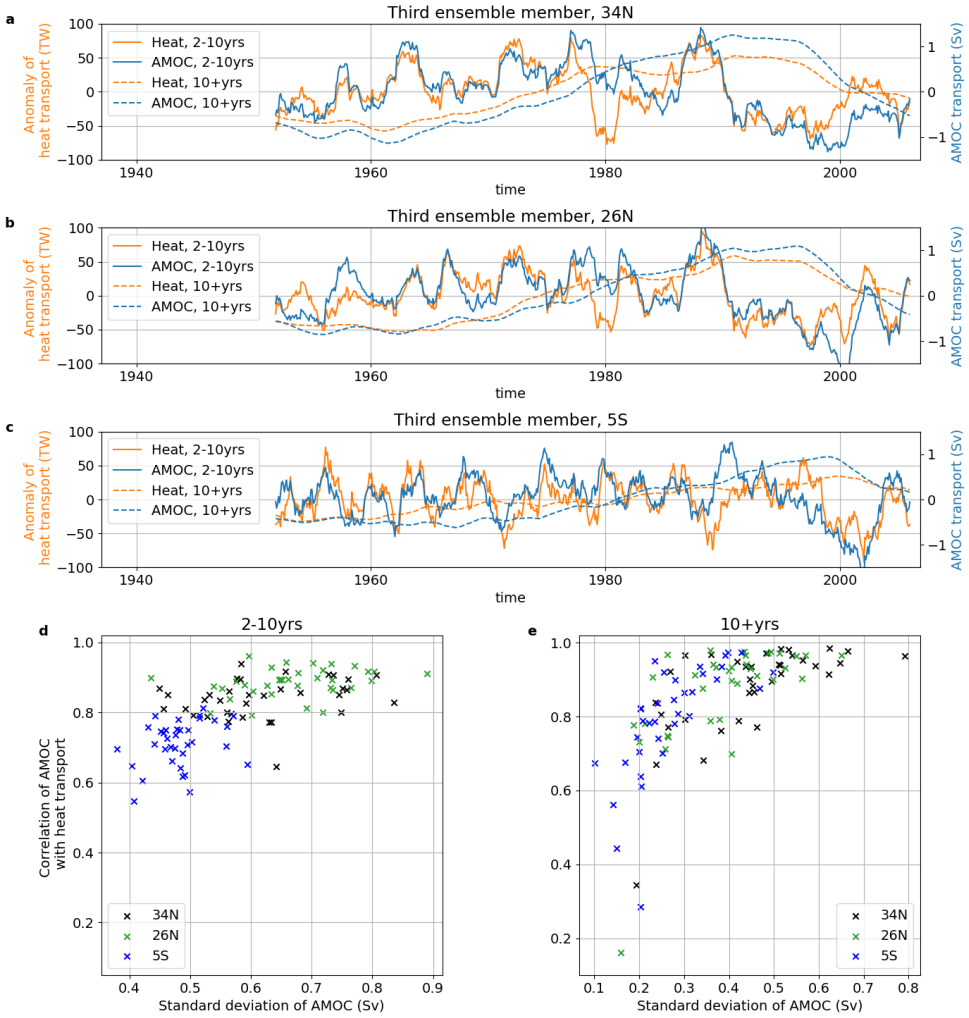

Figure 4. Timeseries of AMOC transport (blue) and heat transport (orange) for the third ensemble member, filtered to pick out variability on 2-10yr timescales (solid lines) and 10+yr timescales (dashed lines) at a) 34°N, b) 26°N and c) 5°S. The correlation between the smoothed heat transport and the smoothed AMOC transport at 34°N, 26°N and 5°S, plotted as a function of the standard deviation of the AMOC, filtered to pick out variability on d) 2-10yr timescales and e) 10+yr timescales (dashed lines). Each cross represents one ensemble member.

Most ensemble members show stronger correlations between AMOC and heat transport at 10+yr timescales than at 2-10yr timescales, consistent with the idea that wind-driven gyre variability is averaged out on timescales larger than 10 years. At all latitudes,

there are stronger correlations between AMOC and OHT in ensemble members with higher AMOC variability.

Given the strong correlation between AMOC and OHT, it should be straightforward to decompose the component of OHT variability driven by AMOC variability. The remainder of this work aims to elucidate the controls on heat transport at these different latitudes and to compare methods for separating northward heat transport by the gyres from northward heat transport by the overturning circulation.

3.3 Heat transport by the gyres vs. heat transport by the overturning

The mean meridional velocity in the first ensemble member at 34°N is shown in figure 5a. The black countour indicates the mean depth of the isopycnal ρ_m and the hatched region is the gyre region used in the streamfunction splitting method. The grey contour indicates the topography. At this latitude, most of the northward flow in the western boundary current is part of the AMOC. Southward flow at depth is not confined to the western boundary, but also occurs on the eastern flank of the mid-Atlantic ridge. The gyre region contains both northward and southward velocities.

The heat transport at 34°N was separated into the heat transport by the net volume transport, the heat transport by the gyres and the heat transport by the overturning circulation using the three methods described in section 2.1. The results are plotted in panels c and d of figure 5. All three methods give significantly different results.

In most ensemble members, the zonal-mean method in z-space attributes about 90% of the heat transport to the overturning at 2-10 yr timescales (green box in figure 5c) and at multidecadal timescales (green box in figure 5d), meaning that the gyre is responsible for about 10% of the heat transport variability. Conceptual arguments suggest that the zonal-mean method in z-space is likely to underestimate the heat transport variability due to AMOC. In the zonal-mean method, the zonal mean temperature is multiplied by the zonal integral of the velocity, even though most of the transport of the AMOC follows the western boundary, where temperatures are much higher. At 34°N, the zonal and depth mean temperature in the top 100m is about 20.2°C. West of 74.5°W (in the western boundary where the AMOC is flowing northward), the zonal and depth mean temperature in the top 100m is about 23.3°C. Hence we expect that the zonal-mean method in z-space underestimates the heat transport variability due to AMOC at 34°N.

The zonal-mean method in density space attributes only about 45% of the heat transport to the overturning on 2-10yr timescales and about 55% of the heat transport to the overturning on 10+yr timescales. This is much lower than the other two methods, again because AMOC variability mostly occurs on the western boundary at this latitude. Isopycnals tilt upwards at the western boundary, and generally the water is warmer here. The zonal average temperature in density space is much lower than the temperature on the western boundary. As a result, the zonal-mean method in density space underestimates the heat transport by the overturning even more than the zonal-mean method in z-space.

Our new method, which we call the western boundary splitting method, is not vulnerable to this problem. It attributes about 94% of the heat transport to the overturning in all ensemble members on 2-10yr timescales and about 120% of the heat transport to the overturning on 10+yr timescales. More heat transport is attributed to AMOC than one might expect based on the correlation between AMOC transport and the total heat transport. The extra variability is compensated by heat transport attributed to the gyre, which is anti-correlated with AMOC transport at 10+yr timescales.

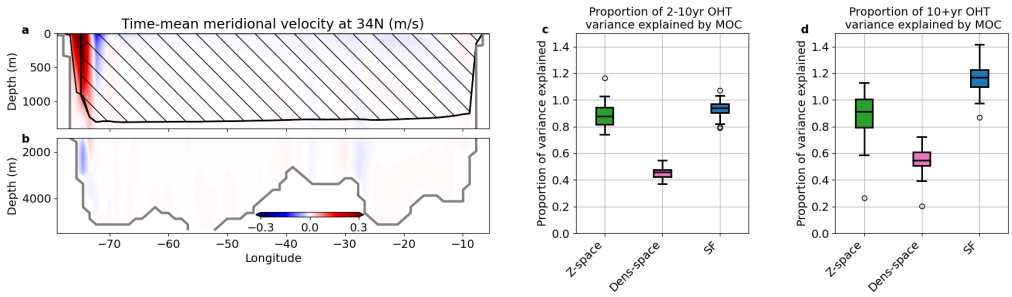

Figure 5. a and b show the time-mean meridional velocity at 34°N for the first ensemble member. The black contour shows the time-mean depth of the isopycnal that passes through the AMOC stream function's maximum. The hatched area is the area associated with the gyre in the streamfunction splitting method. The black vertical line shows the median location of x^*. c) A box and whisker plot of the heat transport on 2-10 yr timescales explained by each method, where the green box represents the proportion of variance explained by AMOC for the zonal-mean method in z space, the pink box represents the proportion of variance explained by AMOC for the zonal-mean method in density space, and the blue box represents the variance explained by AMOC for the streanfunction-splitting method. d) A box and whisker plot of the heat transport on 10+ yr timescales explained by each method (colors as in c).

At 26°N, both the zonal-mean method in z-space and the western boundary splitting method attribute about 100% of the heat transport variability to the AMOC on 2-10yr timescales, while the zonal-mean method in density space attributes only 50% of the heat transport to the AMOC (figure 6c). For the reasons described above, the zonal-mean method in density space under-estimates the part of the heat transport that is performed by the AMOC. On 10+yr timescales, the zonal-mean method in z-space again attributes about 100% of the variability to AMOC, whereas the streamfunction splitting method attributes 120% of variability to AMOC, with some compensation between the AMOC and gyres. Unlike other methods, it is clear what this compensation means in the streamfunction splitting method. Times with high heat transport in the western boundary are associated with times of low heat transport in the gyre region and vice versa. This can easily be explained: when the AMOC transport is larger, more heat is transported northward and temperatures north of 26°N increase, reducing the difference in temperature between northward and southward flowing water in the gyre region.

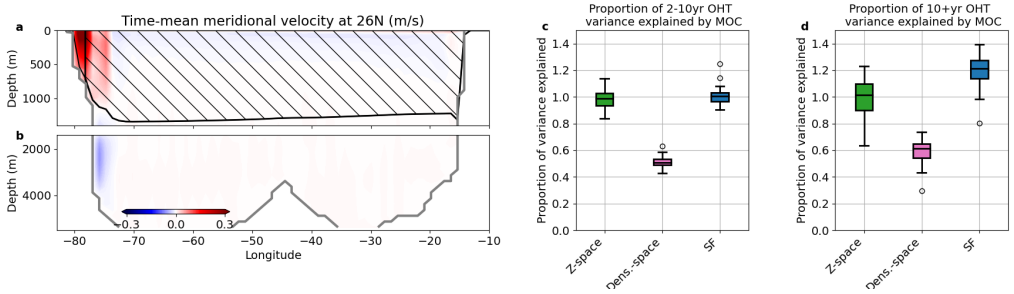

Figure 6. a and b show the time-mean meridional velocity at 26°N for the first ensemble member. The black contour shows the time-mean depth of the isopycnal that passes through the AMOC stream function's maximum. The hatched area is the area associated with the gyre in the streamfunction splitting method. The black vertical line shows the median location of x^*. c) A box and whisker plot of the heat transport on 2-10 yr timescales explained by each method, where the green box represents the proportion of variance explained by AMOC for the zonal-mean method in z space, the pink box represents the proportion of variance explained by AMOC for the zonal-mean method in density space, and the blue box represents the variance explained by AMOC for the streanfunction-splitting method. d) A box and whisker plot of the heat transport on 10+ yr timescales explained by each method (colors as in c).

Because 26°N and 34°N are close together and both occur in the subtropical gyre, we expect that heat transport by the overturning at 26°N and at 34°N are similar to each other, particularly at long timescales. In figure 7, we plot the correlation between the heat transport by the overturning at 26°N and at 34°N for the 2-10yr timescale and for the 10+yr timescale. The zonal-mean method in density space and the streamfunction splitting method both find strong correlations between ocean heat transport attributed to overturning at 26°N and at 34°N, while the zonal-mean method in z-space generally finds weaker correlations between the two latitudes. This is particularly obvious at 10+yr timescales, for which the correlation between 26°N and at 34°N is close to one for the streamfunction splitting method. This suggests that the zonal-mean method in z-space is less robust than the other two methods, and may give different results even at similar latitudes.

At 5°S, the zonal-mean method in z-space attributes about 85% of the heat transport to AMOC on 2-10yr timescales (figure 8c). The zonal-mean method in density space attributes less than 20% of the heat transport to AMOC, again suggesting that this method severely underestimates the role of overturning in heat transport. The streamfunction splitting method attributes about 55% of heat transport variability to AMOC. One reason why the zonal-mean method in z-space and the streamfunction splitting method give such different results is that the zonal-mean method in z-space counts the subtropical cell in the overturning transport. The subtropical cell is primarily a vertical circulation that comprises poleward flow very close to the surface and equatorward flow in the top 100m or so of the water column: because of the strong temperature contrast between these two parts of the flow, the subtropical cell transports a lot of heat. The streamfunction splitting method counts the most of the subtropical cell in the gyre transport, because it takes place away from the western boundary.

At 10+yr timescales, the zonal-mean method in z-space and the streamfunction-splitting method estimate that about 80% of heat transport variability is attributed to the overturning (figure 8d). This is plausible, because the variability of the subtropical cell generally has much shorter timescales. There is a wide variation between ensemble members, possibly caused by low heat transport variability at this latitude on 10+yr timescales. As above, the zonal-mean method in density space severely underestimates the role of overturning in heat transport

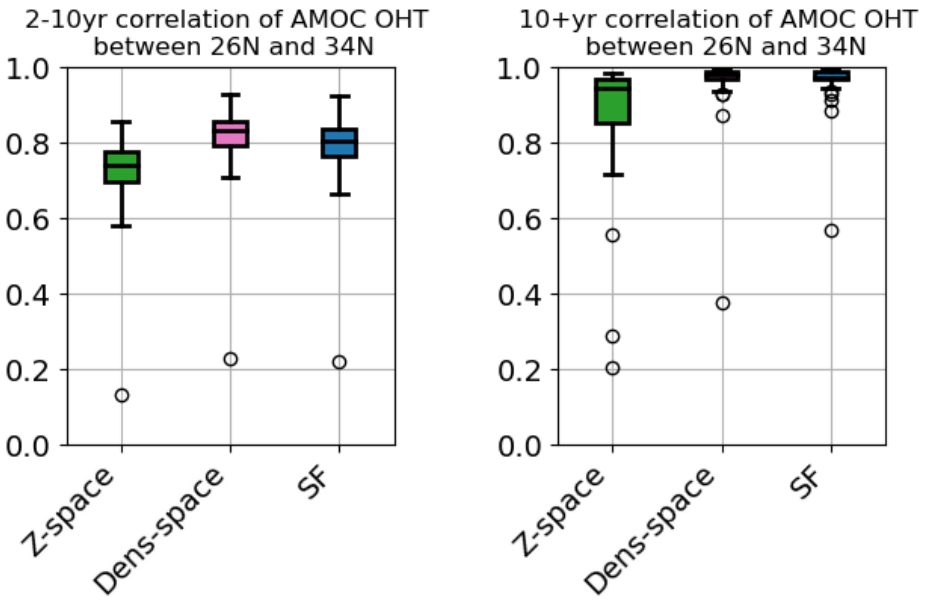

Figure 7. The left panel shows box and whisker plots of the correlation between the ocean heat transport attributed to AMOC at 26°N and at 34°N for each ensemble member, filtered to select 2-10yr timescales. The right panel shows the same, but filtered to select 10+ yr timescales. The green box represents the correlation between OHT explained by AMOC between 26°N and 34°N for the zonal-mean method in z space, the pink box represents the proportion of variance explained by AMOC for the zonal-mean method in density space, and the blue box represents the variance explained by AMOC for the streanfunction-splitting method

4 Conclusions

In this paper, we present three methods for partitioning the AMOC heat transport and the gyre heat transport in the Atlantic basin. The first two methods have been used in the past: both methods estimate the heat transport by the AMOC using the product of the zonal-mean temperature and the zonally-integrated volume transport. The first method takes the zonal mean and zonal integral in depth space: we call this method the zonal-mean method in z-space. The second method takes the zonal mean and zonal integral in density space: we call this method the zonal-mean method in density-space. The third method is a new method which uses physical information about the pathway

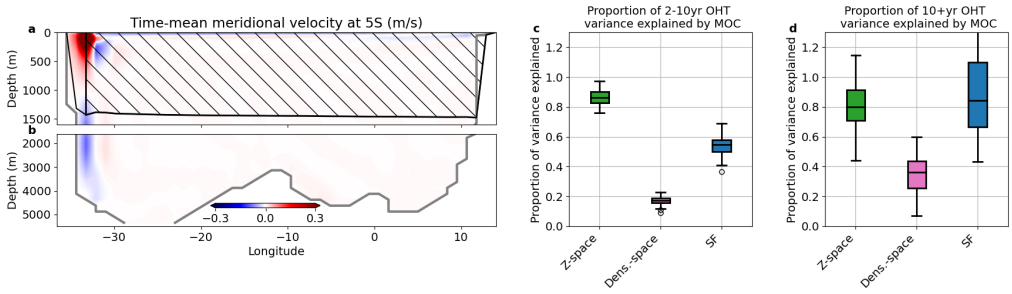

Figure 8. Total heat transport, heat transport by the net volume transport, heat transport by the overturning and heat transport by the gyres at 5°S, for a,c,e the third ensemble member and b,d,f the sixth ensemble member using a, b, the zonal-mean method in z-space, c, d, the zonal-mean method in density space, and e, f the western boundary splitting method. g) A box and whisker plot of the heat transport explained by each method.

of the AMOC to partition the two components of the heat transport. We call this method the streamfunction splitting method.

We compare the methods at three different latitudes: 34°N, 26°N and 5°S. At all of these latitudes, the zonal-mean method in depth space and the zonal-mean method in density space perform very differently from each other. The zonal-mean method in density space always attributes greater than 40% of heat transport to the gyre, and at 5°S, it attributes more than 70% of heat transport to the gyre. Given the strong correlation between AMOC and heat transport at all three latitudes, it seems unlikely that the gyre plays such a large role in heat transport. We find that the zonal-mean method in density space is ineffective for partitioning the heat transport by the overturning and the heat transport by the gyres.

The zonal-mean method in depth space and our new method sometimes give similar results, but at 34°N and at 26°N the zonal-mean method in z-space indicates that 80% to 100% of multidecadal variability is explained by AMOC, with little compensation between the heat transport by the AMOC and the heat transport by the gyres. Like the zonal-mean method in density space, the zonal-mean method in z-space underestimates the heat transport variability due to AMOC because the zonally-integrated temperature is smaller than the temperature of the northward-flowing AMOC transport. Our new streamfunction-splitting method uses recent understanding of AMOC as a circulation in density space, but also applies a new insight: that AMOC follows the western bound-

ary when it flows past clockwise gyre circulations. Hence, our new method does not use a zonal average and is not vulnerable to underestimating AMOC heat transport due to averaging over the whole width of the basin.

The new method presented here indicates that in CESM, heat transport by the AMOC explains about 120% of the multidecadal heat transport variability at 26°N and 34°N (with 20% compensated by southward heat transport in the gyre), and 80% of the heat transport variability at 5°S. Unlike the zonal-mean method in z-space, on long timescales our new method gives very similar results at latitudes that are close to each other. While our new method is difficult to apply directly to observations, it can be applied to any model and a long timeseries is not necessary.

At 5°S, the subtropical cell contributes to the vertical part of the meridional heat transport, but may or may not be considered part of the AMOC. Both the zonal-mean method in z-space and the streamfunction-splitting method are somewhat informative at this latitude: their differences highlight that much of the subtropical cell is found outside the western boundary, and that the subtropical cell is a significant cause of heat transport variability on 2-10yr timescales. Future studies using Lagrangian particles could help ellucidate how the subtropical cell and the upper cell of the AMOC are connected.

5 Open Research

The code repository for this paper is at `https://github.com/cspencerjones/amoc_heat_code`. The data used in this research is the CESM1 Large Ensemble, which is hosted on Amazon Web Services (de La Beaujardiere et al., 2019). This work would not have been possible without the tools provided by and maintained by the Pangeo community (https://pangeo.io/).

Acknowledgments

Thanks to Navid Constantinou for several useful discussions about this work. CSJ's work on this project was supported by NSF award number OCE-2219852.

References

Bhagtani, D., Hogg, A. M., Holmes, R. M., & Constantinou, N. C. (2023). Surface heating steers planetary-scale ocean circulation. *Journal of Physical Oceanog-*

raphy.

Boccaletti, G., Ferrari, R., Adcroft, A., Ferreira, D., & Marshall, J. (2005). The vertical structure of ocean heat transport. *Geophysical Research Letters*, *32*(10).

Borchert, L. F., Müller, W. A., & Baehr, J. (2018). Atlantic ocean heat transport influences interannual-to-decadal surface temperature predictability in the north atlantic region. *Journal of Climate*, *31*(17), 6763–6782.

Bryan, K. (1962). Measurements of meridional heat transport by ocean currents. *Journal of Geophysical Research*, *67*(9), 3403–3414.

Buckley, M. W., & Marshall, J. (2016). Observations, inferences, and mechanisms of the Atlantic Meridional Overturning Circulation: A review. *Reviews of Geophysics*, *54*(1), 5–63.

Cessi, P. (2018). The effect of Northern Hemisphere winds on the meridional overturning circulation and stratification. *Journal of Physical Oceanography*, *48*(10), 2495–2506.

de La Beaujardiere, J., Banihirwe, A., Shih, C., Paul, K., & Hamman, J. (2019). NCAR CESM LENS cloud-optimized subset. *UCAR/NCAR Computational and Informations Systems Lab*. doi: 10.26024/wt24-5j82

Eden, C., & Willebrand, J. (2001). Mechanism of interannual to decadal variability of the North Atlantic circulation. *Journal of Climate*, *14*(10), 2266–2280.

Ferrari, R., & Ferreira, D. (2011). What processes drive the ocean heat transport? *Ocean Modelling*, *38*(3-4), 171–186.

Folland, C. K., Palmer, T. N., & Parker, D. E. (1986). Sahel rainfall and worldwide sea temperatures, 1901–85. *Nature*, *320*(6063), 602–607.

Foukal, N. P., & Chafik, L. (2022). The AMOC needs a universally-accepted definition. *Authorea Preprints*.

Goldenberg, S. B., Landsea, C. W., Mestas-Nuñez, A. M., & Gray, W. M. (2001). The recent increase in Atlantic hurricane activity: Causes and implications. *Science*, *293*(5529), 474–479.

Gray, A. R., & Riser, S. C. (2014). A global analysis of Sverdrup balance using absolute geostrophic velocities from Argo. *Journal of Physical Oceanography*, *44*(4), 1213–1229.

Hall, M. M., & Bryden, H. L. (1982). Direct estimates and mechanisms of ocean heat transport. *Deep Sea Research Part A. Oceanographic Research Papers*,

29(3), 339–359.

Jackson, L., Kahana, R., Graham, T., Ringer, M., Woollings, T., Mecking, J., & Wood, R. (2015). Global and European climate impacts of a slowdown of the AMOC in a high resolution GCM. *Climate dynamics*, *45*, 3299–3316.

Jones, C., & Cessi, P. (2018). Components of upper-ocean salt transport by the gyres and the meridional overturning circulation. *Journal of Physical Oceanography*, *48*(10), 2445–2456.

Kang, S. M., Frierson, D. M., & Held, I. M. (2009). The tropical response to extratropical thermal forcing in an idealized GCM: The importance of radiative feedbacks and convective parameterization. *Journal of the atmospheric sciences*, *66*(9), 2812–2827.

Kay, J. E., Deser, C., Phillips, A., Mai, A., Hannay, C., Strand, G., ... others (2015). The Community Earth System Model (CESM) large ensemble project: A community resource for studying climate change in the presence of internal climate variability. *Bulletin of the American Meteorological Society*, *96*(8), 1333–1349.

Klotzbach, P., Gray, W., & Fogarty, C. (2015). Active Atlantic hurricane era at its end? *Nature Geoscience*, *8*(10), 737–738.

Larson, S. M., Buckley, M. W., & Clement, A. C. (2020). Extracting the buoyancy-driven Atlantic meridional overturning circulation. *Journal of Climate*, *33*(11), 4697–4714.

Marshall, J., Donohoe, A., Ferreira, D., & McGee, D. (2014). The ocean's role in setting the mean position of the Inter-Tropical Convergence Zone. *Climate Dynamics*, *42*, 1967–1979.

Martin, E. R., & Thorncroft, C. D. (2014). The impact of the AMO on the West African monsoon annual cycle. *Quarterly Journal of the Royal Meteorological Society*, *140*(678), 31–46.

McDonagh, E. L., McLeod, P., King, B. A., Bryden, H. L., & Valdés, S. T. (2010). Circulation, heat, and freshwater transport at 36 N in the Atlantic. *Journal of physical oceanography*, *40*(12), 2661–2678.

Oldenburg, D., Wills, R. C., Armour, K. C., Thompson, L., & Jackson, L. C. (2021). Mechanisms of low-frequency variability in North Atlantic Ocean heat transport and AMOC. *Journal of Climate*, *34*(12), 4733–4755.

Pickart, R. S., & Spall, M. A. (2007). Impact of Labrador Sea convection on the North Atlantic meridional overturning circulation. *Journal of Physical Oceanography*, *37*(9), 2207–2227.

Piecuch, C. G., Ponte, R. M., Little, C. M., Buckley, M. W., & Fukumori, I. (2017). Mechanisms underlying recent decadal changes in subpolar North Alantic Ocean heat content. *Journal of Geophysical Research: Oceans*, *122*(9), 7181–7197.

Roemmich, D., & Wunsch, C. (1985). Two transatlantic sections: Meridional circulation and heat flux in the subtropical North Atlantic Ocean. *Deep Sea Research Part A. Oceanographic Research Papers*, *32*(6), 619–664.

Rypina, I. I., Pratt, L. J., & Lozier, M. S. (2011). Near-surface transport pathways in the North Atlantic Ocean: Looking for throughput from the subtropical to the subpolar gyre. *Journal of Physical Oceanography*, *41*(5), 911–925.

Stommel, H. (1957). A survey of ocean current theory. *Deep Sea Research (1953)*, *4*, 149–184.

Talley, L. D. (1999). Some aspects of ocean heat transport by the shallow, intermediate and deep overturning circulations. *Geophysical Monograph-American Geophysical Union*, *112*, 1–22.

Trenberth, K. E., & Fasullo, J. T. (2017). Atlantic meridional heat transports computed from balancing earth's energy locally. *Geophysical Research Letters*, *44*(4), 1919–1927.

Warren, B. A. (1999). Approximating the energy transport across oceanic sections. *Journal of Geophysical Research: Oceans*, *104*(C4), 7915–7919.

Yan, X., Zhang, R., & Knutson, T. R. (2018). Underestimated AMOC variability and implications for AMV and predictability in CMIP models. *Geophysical Research Letters*, *45*(9), 4319–4328.

Yang, J. (2015). Local and remote wind stress forcing of the seasonal variability of the Atlantic Meridional Overturning Circulation (AMOC) transport at 26.5 N. *Journal of Geophysical Research: Oceans*, *120*(4), 2488–2503.

Yeager, S. G., Karspeck, A. R., & Danabasoglu, G. (2015). Predicted slowdown in the rate of Atlantic sea ice loss. *Geophysical Research Letters*, *42*(24), 10–704.

Young, W. R. (2012). An exact thickness-weighted average formulation of the Boussinesq equations. *Journal of Physical Oceanography*, *42*(5), 692–707.

Zhang, R., Sutton, R., Danabasoglu, G., Kwon, Y.-O., Marsh, R., Yeager, S. G., ... Little, C. M. (2019). A review of the role of the Atlantic meridional overturning circulation in Atlantic multidecadal variability and associated climate impacts. *Reviews of Geophysics*, *57*(2), 316–375.

Zhang, R., & Thomas, M. (2021). Horizontal circulation across density surfaces contributes substantially to the long-term mean northern Atlantic Meridional Overturning Circulation. *Communications Earth & Environment*, *2*(1), 112.